# Satellite Ground Stations with Electronic Beam Steering

*Yao Cheng*, *Nuan Song*, *Florian Roemer*, *Martin Haardt*
Communications Research Laboratory
Ilmenau University of Technology
Ilmenau, Germany
{y.cheng, nuan.song, florian.roemer, martin.haardt}@tu-ilmenau.de

*Hennes Henniger*, *Robert Metzig*, *Erhard Diedrich*
German Aerospace Center (DLR)
Oberpfaffenhofen, Germany
{hennes.henniger, robert.metzig, erhard.diedrich}@dlr.de

***Abstract*—In this work, we propose electronic beam steering via antenna arrays as a substitute for large parabolic antennas at satellite ground stations. We concentrate on two array geometries, faceted arrays and hemispherical arrays. A thorough analysis is carried out of the radiation characteristics, the array size, as well as the antenna element distribution and spacing. Moreover, in order to fulfill the requirement of the array design, that is, to achieve a higher gain at low elevation angles where the longer spacecraft to ground station distance leads to a larger range loss, we propose to adjust the number of active antenna elements, i.e., some antenna elements are turned on while others are turned off according to the required level of antenna gain. This also contributes to a concept of an optimized array design for this specific application. In the simulations, the array optimization for both array geometries is further investigated and realized with a realistic ephemeris incorporated. The numerical results support the proposal of replacing large reflector antennas by electronic beam steering via antenna arrays at satellite ground stations.**

## I. Introduction

Nowadays, payload data from earth-observation low-earth orbiting (LEO) satellites is received by mechanically steered large aperture parabolic tracking antennas. On the one hand, parabolic tracking antennas achieve a good directivity. On the other hand, pointing the narrow beam towards the spacecraft is very challenging, especially considering the large weight and the high wind-load of the antenna structure. The requirement for frequent maintenance due to the effect of extreme weather conditions especially for polar stations and the physical limitations of the steering devices make mechanical steering a technically challenging and cost-intensive approach. These issues with the mechanical steering give rise to the need of a search for an alternative.

We propose to find a replacement of the mechanical steering by resorting to electronic beam steering via antenna arrays. Each of the antenna elements in the array is equipped with its own RF chain and its own analog/digital (AD) converter. Therefore, spacecraft tracking, interference suppression, and even the separation of signals from multiple spacecraft can be achieved by performing signal processing in the digital domain such that the mechanical steering is completely avoided and flexibility in combating interference is acquired. Moreover, exploiting the array geometry and size as well as the distribution and the electrical properties of the antenna elements leads to a high gain.

In the 1960s, many researchers have started to investigate potential setups of antenna arrays to achieve the coverage of an upper hemisphere. In [1], it is concluded that to realize electronic beam scanning of a hemisphere, a phased array antenna with a minimum of 3 faces is required, and using 4 (cf. Fig. 2), 5 (cf. Fig. 4) or 6 faces, the performance of the antenna array is improved in terms of the maximum scan angle and the scan loss. Later in [2], a more comprehensive study of an antenna array system comprising several planar arrays each tilted to jointly provide the coverage of a hemisphere is presented. The problem of determining the minimum value of the maximum scan angle and the tilting angles of the faces of the antenna array is solved analytically with the aid of coordinate transformations. Both [1] and [2] serve as a good starting point of the investigations on the so-called faceted arrays by presenting the basic designing criteria of such antenna arrays and a method of approximately determining the array size to achieve a required array gain. However, these works focus more on the geometrical setup of faceted arrays, while the radiation characteristics of faceted arrays are not discussed, i.e., what the beam patterns of faceted arrays are like with different types of antenna elements adopted. Besides faceted arrays, antenna arrays with a hemispherical geometry have received much research attention as well. In [6], some general conventions for the investigations on spherical arrays are presented. The authors of [5] further study the radiation properties of a spherical antenna array with a limited number of omnidirectional antenna elements. These works present the methodology of analyzing a spherical or hemispherical antenna array and make the potentials of such an array geometry in the application of electronic beam steering more convincing.

Inspired by these pioneering works, in the search for candidate array geometries, we focus on faceted arrays and hemispherical arrays, and carry out a thorough analysis of the radiation characteristics, array size, antenna element distribution and spacing. A system model of electronic beam steering via antenna arrays is constructed to aid the studies of the beam

patterns. It can also be used to facilitate future extensions, such as the interference suppression and multi-mission support which means receiving signals from more than one spacecraft at a time.

Note that at low elevation angles, due to a larger range loss caused by the longer spacecraft to ground station distance, a greater antenna gain is demanded. In order to achieve this goal of the array design, we propose to adjust the number of active antenna elements according to the required level of antenna gain. Based on this idea, the array design for this specific application of employing electronic beam steering at ground stations for the reception of payload from LEO satellites is optimized. Simulations are then performed to further investigate the array optimization and prove the concept of replacing large reflector antennas by electronic beam steering via antenna arrays. The TerraSAR-X satellite is used as a reference mission. With the aid of AGI's Satellite Took Kit (STK) software, we obtain the spacecraft flight paths and include them into our simulations as well.

The remainder of the paper is organized as follows. In Section II, we introduce the system model where electronic beam steering is employed. With a focus on two array geometries, faceted arrays and hemispherical arrays, the calculations of the array manifolds and the analysis of the element distributions and spacings are presented in Section III. Section IV provides more insights into the array optimization for the application of employing electronic beam steering at the ground stations. The simulation results are presented in Section V.

## II. System Model of Electronic Beam Steering

Considering an antenna array with $M$ antenna elements, its array manifold is written as

$$\boldsymbol{a}(\theta,\phi) = \begin{bmatrix} a_1 & a_2 & \dots & a_M \end{bmatrix}^{\mathrm{T}} \in \mathbb{C}^{M\times 1}, \tag{1}$$

with

$$a_i = g_i(\theta,\phi)\cdot e^{j\frac{2\pi}{\lambda}\boldsymbol{r}^{\mathrm{T}}\cdot\boldsymbol{r}_i}, \quad i=1,2,\dots,M,$$

where $\boldsymbol{r}_i$ is the spatial location vector of the $i$-th antenna element, $\boldsymbol{r}$ is the unit vector pointing to the direction $(\theta,\phi)$ as represented in a right-handed spherical coordinate system depicted in Fig. 1, and $g_i(\theta,\phi)$ is the complex gain of the $i$-th antenna element. Here $\lambda$ denotes the wavelength. In the analysis of various array geometries, it is common to define two coordinate systems, one for the whole antenna array system and the coverage, and one for the active area or each of the active antenna elements. Therefore, two sets of coordinates are used: $(x,y,z;r,\theta,\phi)$ for the array system and its coverage, $(x_0,y_0,z_0;r_0,\theta_0,\phi_0)$ for the active area or the active antenna elements. Note that as the coverage of an upper hemisphere is considered, the ranges of the azimuth angle $\phi$ and the co-elevation angle $\theta$ of interest are $0^\circ \le \phi < 360^\circ$ and $0^\circ \le \theta \le 90^\circ$, respectively.

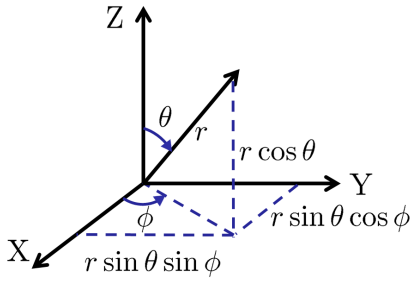

Fig. 1. Definition of the spherical coordinate system

First, let us consider the local coordinate system of each antenna element. In the active area of an antenna array, the spatial location vector of the $i$-th antenna element with the coordinates $(x_{0,i},y_{0,i},z_{0,i})$, is written as

$$\boldsymbol{r}_i = x_{0,i}\cdot\boldsymbol{e}_{x,0} + y_{0,i}\cdot\boldsymbol{e}_{y,0} + z_{0,i}\cdot\boldsymbol{e}_{z,0}, \tag{2}$$

where $\boldsymbol{e}_{x,0}$, $\boldsymbol{e}_{y,0}$, and $\boldsymbol{e}_{z,0}$ are the unit vectors in the directions of the X-axis, Y-axis, and Z-axis of the local coordinate system, respectively. The unit vector pointing to direction $(\theta,\phi)$ can be expressed considering the local coordinate system of the $i$-th antenna element as

$$\boldsymbol{r} = \sin\theta_{0,i}\cdot\cos\phi_{0,i}\cdot\boldsymbol{e}_{x,0} + \sin\theta_{0,i}\cdot\sin\phi_{0,i}\cdot\boldsymbol{e}_{y,0} + \cos\theta_{0,i}\cdot\boldsymbol{e}_{z,0} \tag{3}$$

where $(\theta_{0,i},\phi_{0,i})$ is the direction $(\theta,\phi)$ observed in the local coordinate system. Note that $(\theta_{0,i},\phi_{0,i})$ can be represented by $(\theta,\phi)$ using coordinate transformations which are detailed in Section III for different array geometries considered in this work.

The Bartlett beamformer [3] is employed to steer the beam to the direction $(\theta_{\mathrm{sat}},\phi_{\mathrm{sat}})$, which is expressed as

$$\boldsymbol{w} = \begin{bmatrix} w_1 & w_2 & \dots & w_M \end{bmatrix}^{\mathrm{T}} \in \mathbb{C}^{M\times 1} \tag{4}$$

with

$$w_i = \frac{1}{\sqrt{M}} e^{j\frac{2\pi}{\lambda}\boldsymbol{r}_{\mathrm{sat}}^{\mathrm{T}}\cdot\boldsymbol{r}_i}, \quad i=1,2,\dots M$$

where $\boldsymbol{r}_{\mathrm{sat}}$ is the vector pointing to the direction $(\theta_{\mathrm{sat}},\phi_{\mathrm{sat}})$. The Bartlett beamformer can be seen as the spatial equivalent of a matched filter. The beam pattern of a beamformer is written as

$$P(\theta,\phi) = |\boldsymbol{w}^{\mathrm{H}}\cdot\boldsymbol{a}|^2, \tag{5}$$

which measures the power radiated towards direction $(\theta,\phi)$.

## III. Array Geometries

According to a typical link budget for an X-band downlink from a LEO spacecraft, besides covering the whole range of the elevation angles, the designed antenna array must achieve a higher gain at low elevation angles. Based on this prerequisite, planar arrays are excluded from the candidate set of antenna arrays. It is due to the fact that the effective aperture of planar arrays decreases for low elevations. Thus they cannot provide high gains in this region and consequently suffer from limited coverage. Nevertheless, faceted arrays [1] are of interest, where several planar arrays are tilted at a specific angle to jointly provide the coverage of a full upper hemisphere. When it comes to the arrangement of antenna elements on the planar array on each surface of the faceted array, the triangular lattice or the so called triangular spacing [2] and the rectangular

spacing [2] (cf. Fig. 3) as in the uniform rectangular array are considered. Furthermore, mounting antenna elements on a curved surface [4], such as a hemisphere, is also an option.

### A. Faceted arrays

In Fig. 2, a geometrical illustration of the coverage of a 4-face faceted array is presented. Each of the 4 faces provides the coverage of a quarter of an upper hemisphere. Using the frontal face of this faceted array as an example, the projection of its coverage area on a hemisphere onto the X-Y plane is a circular sector with a central angle of $90°$. The angle between the zenith of the array system and the normal of the frontal face, i.e., the boresight of the frontal sub-array as referred to in Fig. 2, is defined as the maximum scan angle, denoted as $\theta_{s,\max}$ in Fig. 2. Note that the angles between the boresight of the frontal sub-array and the two edges (radius) of the sector are both equal to $\theta_{s,\max}$ as well [2], as depicted in Fig. 2.

With the far field assumption, the coordinate system of the array system and that of each active antenna element share a common origin. Therefore, the local coordinate system of the frontal face is obtained by rotating the array coordinate system with respect to the Y-axis by $\beta_2$ following the right-hand grip rule. Indexing the 4 faces counter-clockwise starting from the frontal face, it is observed that the local coordinate system of face 2 is obtained by first rotating the array coordinate system with respect to the Z-axis by $\beta_1$, and then rotating the resulting one with respect to its Y-axis by $\beta_2$, both following the right-hand grip rule. The rotation angles and the coverage regions

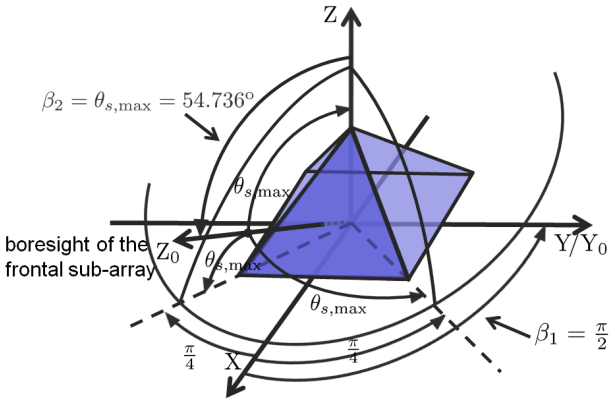


Fig. 2. Geometrical illustration of the coverage of a 4-face faceted array using the frontal face as an example

of the sub-arrays of a 4-face faceted array are summarized in Table I. It should be noted that faceted arrays with a top face or the so-called zenith face whose normal overlaps with the Z-axis of the array coordinate system are also of interest. Using a 5-face faceted array with a zenith face as an example, we present the rotation angles and the coverage regions of its sub-arrays in Table II. Note that the zenith face has the index of 5.

When performing electronic beam steering using a faceted array, the antenna elements of a sub-array are switched on when the current direction of the spacecraft $(\theta_{\text{sat}}, \phi_{\text{sat}})$ fits in its coverage area in terms of the ranges of $\phi$ and $\theta$ as

TABLE I
ROTATION ANGLES AND COVERAGE REGIONS OF THE SUB-ARRAYS OF A 4-FACE FACETED ARRAY

| face | $\beta_1$ | $\beta_2$ | coverage - $\phi$ | coverage - $\theta$ |
|---|---|---|---|---|
| 1 | $0°$ | $54.736°$ [2] | $0° \to 45°$ and $315° \to 360°$ | $0° \to 90°$ |
| 2 | $90°$ | | $45° \to 135°$ | |
| 3 | $180°$ | | $135° \to 225°$ | |
| 4 | $270°$ | | $225° \to 315°$ | |

TABLE II
ROTATION ANGLES AND COVERAGE REGIONS OF THE SUB-ARRAYS OF A 5-FACE FACETED ARRAY WITH A ZENITH FACE

| face | $\beta_1$ | $\beta_2$ | coverage - $\phi$ | coverage - $\theta$ |
|---|---|---|---|---|
| 1 | $0°$ | $74.458°$ [2] | $0° \to 45°$ and $315° \to 360°$ | $47.059° \to 90°$ |
| 2 | $90°$ | | $45° \to 135°$ | |
| 3 | $180°$ | | $135° \to 225°$ | |
| 4 | $270°$ | | $225° \to 315°$ | |
| 5 | $0°$ | $0°$ | $0° \to 360°$ | $0° \to 47.059°$ |

shown in Table I and II. Therefore, in the single mission case, where a faceted array equipped at the ground station is in charge of the reception of signals from a single spacecraft, only one sub-array of this faceted array is set active. On the other hand, in a multi-mission scenario, more than one sub-array will be switched on to form multiple beams and to realize the reception of data from several spacecrafts simultaneously.

*1) Array manifold:* Consider an active face of a faceted array, all $M_0$ antenna elements are located on the X-Y plane of the local coordinate system. Recalling (2), the spatial location vector of the $i$-th antenna element with the coordinate $(x_{0,i}, y_{0,i}, 0)$, is written as

$$\boldsymbol{r}_i = x_{0,i} \cdot \boldsymbol{e}_{x,0} + y_{0,i} \cdot \boldsymbol{e}_{y,0}. \tag{6}$$

Based on the far field assumption and the fact that all the antenna elements on the active face share the same local coordinate system, i.e., the coordinate system of the active face, the following can be obtained

$$\theta_0 = \theta_{0,1} = \theta_{0,2} = \ldots = \theta_{0,M_0} = f(\theta, \phi)$$

$$\phi_0 = \phi_{0,1} = \phi_{0,2} = \ldots = \phi_{0,M_0} = h(\theta, \phi)$$

$$g_1(\theta_{0,1}, \phi_{0,1}) = \ldots = g_{M_0}(\theta_{0,M_0}, \phi_{0,M_0}) = g(\theta_0, \phi_0)$$

where the transformation from $(\theta, \phi)$ to $(\theta_0, \phi_0)$ is achieved by

$$f(\theta, \phi) = \arccos\left(\cos\beta_2 \cdot \cos\theta + \sin\beta_2 \cdot \sin\theta \cdot \cos\left(\phi - \beta_1\right)\right), \tag{7}$$

$$h(\theta, \phi) = \arctan2\big(\sin\theta \cdot \sin\left(\phi - \beta_1\right), \cos\beta_2 \cdot \sin\theta \cdot \cos\left(\phi - \beta_1\right) - \sin\beta_2 \cdot \cos\theta\big). \tag{8}$$

Here the two-argument function arctan2 is a variation of the arctangent function. By using arctan2, the signs of its two arguments are taken into account to avoid the ambiguity involved in deciding between two angles with a difference of $\pi$ caused by adopting the arctangent function. Note that the rotation angles $\beta_1$ and $\beta_2$ are defined as in the previous text. The $i$-th entry of the vector representing the array manifold is therefore written as

$$a_i = g(\theta_0, \phi_0) \cdot e^{j\frac{2\pi}{\lambda}(x_{0,i}\cdot\sin\theta_0\cdot\cos\phi_0 + y_{0,i}\cdot\sin\theta_0\cdot\sin\phi_0)}. \quad (9)$$

*2) Antenna element distribution and spacing:* The rectangular spacing and the triangular spacing are considered as two types of antenna element distributions for faceted arrays. An illustration together with the notations of the element spacings are presented in Fig. 3. Generally speaking, a larger element

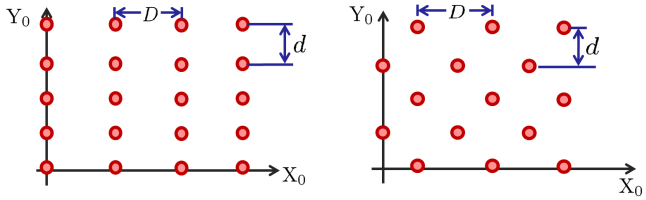


Fig. 3. Rectangular spacing and triangular spacing

spacing is preferred, considering the reduced packaging and fabrication difficulties or a higher gain resulting from a bigger array aperture area. However, it is well known that for planar arrays with a rectangular spacing, an element spacing larger than half the wavelength $\lambda$ causes grating lobes. To avoid the occurrence of grating lobes, the restrictions on the element spacings are: $D \leq \frac{\lambda}{2}$ and $d \leq \frac{\lambda}{2}$. It is indicated in [7] that for a planar array the element spacing can be increased as long as the borders of the regions of the grating lobes do not surpass that of the coverage region of the array. This can also be applied to the sub-arrays of a faceted array [2], i.e., the element spacing can be increased only to ensure that the emergence of the grating lobes is avoided in the coverage of the sub-arrays. The coverage region and grating lobe regions of a sub-array of a 5-face faceted array with a zenith face are shown in Fig. 4, where the geometric setup of such a faceted array is also depicted. Note that here the local coordinate system of a sub-array is adopted for the plotting of the coverage region and the grating lobe regions. In this example, the antenna elements are displaced on a equilateral triangular lattice. Here, since the end-fire ($\theta_0 = 90°$) is not in the coverage of any sub-array of a faceted array, the grating lobes are allowed at the end-fire, and the element spacings are: $D = 0.679\lambda$ and $d = 0.588\lambda$. It should be noted that by increasing the number of sub-arrays of a faceted array, the coverage region of each sub-array is then reduced, which brings in the benefit of a larger allowed element spacing.

### B. Hemispherical arrays

*1) Array manifold:* Let us consider a hemispherical array with the radius $R$, which is depicted in Fig. 5. The location of the $i$-th active element on the array is specified by its spherical coordinate $(\beta_{1,i}, \beta_{2,i}, R)$. Note that $(\beta_{1,i}, \beta_{2,i})$ also defines the

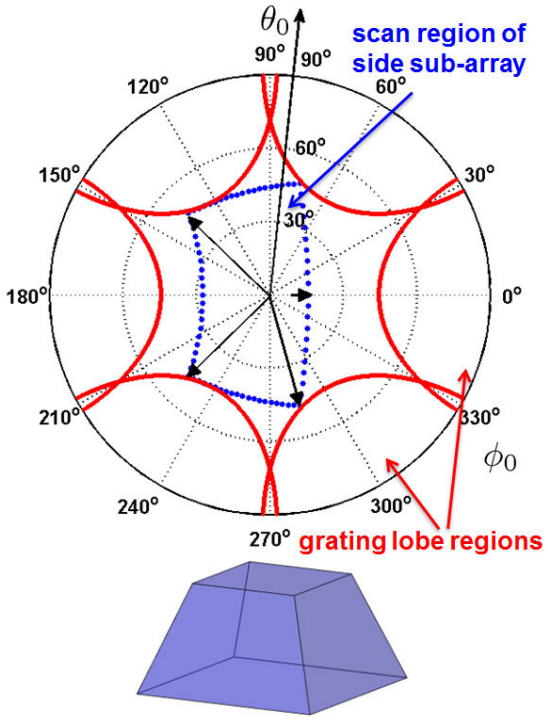


Fig. 4. Coverage region, grating lobe regions, illustration of the geometric setup of a 5-face faceted array with a zenith face

direction of the Z-axis in the local coordinate system of the $i$-th active element and specifies the rotation angles in the transformation from the coordinate system of the array to the local one. We can then express the spatial location vector of the $i$-th antenna element as

$$\boldsymbol{r}_i = R \cdot \boldsymbol{e}_{z,0}. \quad (10)$$

Therefore, the $i$-th entry of the vector representing the array manifold of a hemispherical array is written as

$$a_i = g_i(\theta_{0,i}, \phi_{0,i}) \cdot e^{j\frac{2\pi}{\lambda}(R\cdot\cos\theta_{0,i})}. \quad (11)$$

Note that the transformation from $(\theta, \phi)$ to $(\theta_{0,i}, \phi_{0,i})$ can also be carried out using (7) and (8) with the rotation angles of the $i$-th active antenna element $\beta_{1,i}$ and $\beta_{2,i}$.

For a hemispherical antenna array, a maximum coverage angle $\theta_{\text{cov}}$ ranging from $0°$ to $90°$ is introduced to determine whether an antenna element is active or not [5]. Therefore, for the $j$-th antenna element, considering its local coordinate system, its coverage area characterized by the co-elevation angle $\theta_{0,j}$ is then $0° \leq \theta_{0,j} \leq \theta_{\text{cov}}$. When performing electronic beam steering via a hemispherical antenna array, if the direction of the spacecraft transformed into the coordinate system of the $j$-th antenna element fits into the aforementioned range of coverage, this antenna element is switched on; otherwise, it is switched off. The reason why such a procedure is introduced to selectively switch on some antenna elements instead of using all is three-fold. First, this mechanism brings in more degrees of freedom in the adaptation of the antenna gain. Imagine building up a hemispherical antenna array with a large number of antenna elements, by adjusting the number of active ones, different levels of antenna gain can be provided, adapting to

different requirements of various missions. Second, according to a required antenna gain, shutting off some antenna elements reduces the complexity involved in the beamforming network as well as avoiding an unnecessary margin. Third, switching off some antenna elements which unnecessarily stay active contributing to the signal reception avoids bringing noise in. Thus, the noise level at the receiver is reduced.

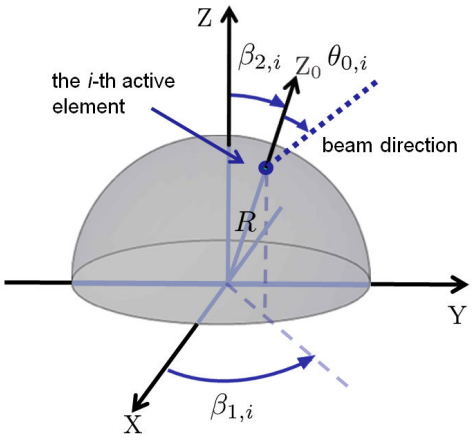


Fig. 5. Illustration of a hemispherical array

*2) Antenna element distribution and spacing:* To generate a nearly uniform distribution of antenna elements on a hemispherical array, we adopt the idea of constructing a geodesic sphere starting from an icosahedron [9]. First, each edge of an icosahedron is bisected, and the dots are connected and popped out to a sphere circumscribed around the icosahedron. Next, the same procedures are carried out to the polyhedron obtained from previous steps until the number of points on the polyhedron contacting the sphere approaches the required array size. The locations of these contacting points then represent the distribution of the antenna elements. Note that, for a hemispherical array, there exist more degrees of freedom in determining the element spacing. The spherical surface, unlike a planar one, relieves the half wavelength constraint on the element spacing. However, it should be noted that, if the element spacing is too large, the so-called pseudo grating lobes [5] will be caused.

*3) Practical considerations:* Although the hemispherical geometry does look intuitive when it comes to the design of an antenna array to achieve the coverage of a hemisphere, mounting antenna elements on a curved surface is challenging in practice. Recently, the idea of geodesic dome antenna arrays has been proposed [8], which allows keeping the array architecture locally planar and globally approximately spherical. A geodesic array comprises sub-arrays on flat panels which are assembled to form the hemispherical structure. In this way, the huge fabrication complexity which is the bottleneck of the realization of curved arrays is avoided by resorting to the already mature fabrication techniques for planar arrays.

## IV. Array Optimization

In general, for receiving a signal from LEO satellite dumping its data to a ground station, the received power flux density is reciprocal to the square of the link distance. For a typical ephemeris of LEO satellites, the link distance between the acquisition of signal (AOS) and the loss off signal (LOS) varies between approximately 2000 km and 500 km, depending on the orbit height and the current elevation angle from the ground station to the satellite. Assuming an omnidirectional antenna pattern at the spacecraft, this fact requires higher antenna gains at lower elevation angles on the ground station. For a classic high gain tracking antenna, the gain is constant over the elevation and cannot be adapted. This optimization can only be solved using electronic beam steering. For both faceted arrays and hemispherical arrays, the number of active antenna elements can be adjusted. In the case of the faceted arrays, more antenna elements are switched on at low elevation angles and for a higher elevation angle, fewer antenna elements are kept active according to the required level of antenna gain. When it comes to the case of hemispherical arrays or geodesic arrays, as introduced in Section III-B, the active area or the number of active antenna elements is determined by the maximum coverage angle. Thus, setting a larger maximum coverage angle leads to a higher gain, which fulfills the requirement of the array design. In Section V, the gain optimization fitting to the predicted range-loss is investigated by means of simulations.

## V. Simulations

In Fig. 6 the normalized variation of the range-loss versus the elevation angle for an ascending TerraSAR-X contact over the ground station Kiruna is presented. Range values are retrieved from a real TerraSAR-X contact, with the aid of AGI's Satellite Took Kit (STK) software. TerraSAR-X orbits the Earth in a 514 km Sun-synchronous dusk-dawn orbit with a 97° inclination and an 11 day repeat period. The elevation scale ranges from the AOS at 0° elevation to the maximum elevation angle of 82° of this dedicated exemplary high-elevation contact. X-band transmissions on a frequency of 8.15 GHz are assumed.

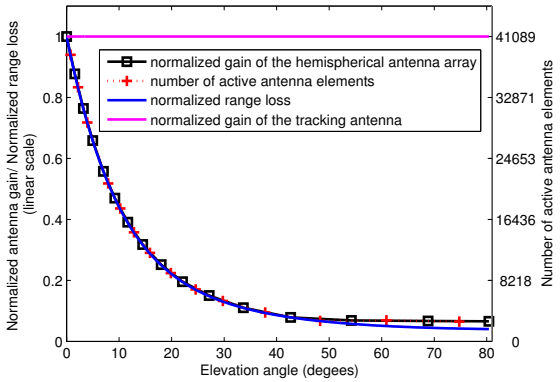


Fig. 6. Normalized array gain of a hemispherical array with 82177 antenna elements in total and the number of active antenna elements adjusted according to the normalized range loss

The horizontal line in Fig. 6 represents the normalized gain of a tracking antenna. As perfect tracking is assumed, the tracking antenna provides a constant gain over all the elevation angles. The aperture of the tracking antenna is determined

by the required gain at the AOS at $0^\circ$ elevation which is assumed to be $46$ dBi. It can be seen that the design of the tracking antenna is made on a worst case assumption. Taking into account that the range loss decreases with the elevation, it can be seen that the system will show an unnecessary margin of up to $13.9$ dB.

Fig. 6 shows further the normalized antenna gain of a hemispherical electronic beam steering array. In total, $82177$ omnidirectional antenna elements are mounted on this hemispherical array with a radius of approximately $57.8\lambda$, such that at $0^\circ$ elevation with a maximum coverage angle $\theta_{\text{cov}} = 90^\circ$, the required antenna gain of $46$ dBi is achieved. Note that the mechanism of selecting active antenna elements results in the fact that with a constant maximum coverage angle $\theta_{\text{cov}}$, antenna elements located on a surface centered at the spacecraft direction and angular size of $2\theta_{\text{cov}}$ are switched on as depicted in the left part of Fig. 7. Hence, due to

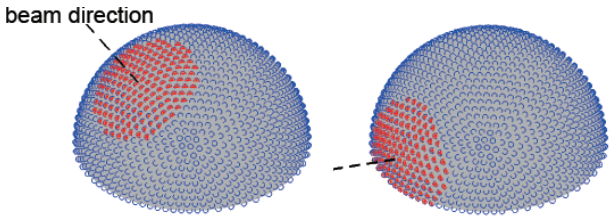


Fig. 7. Illustration of the selection of the active antenna elements (in red) on a hemispherical array with $\theta_{\text{cov}} = 30^\circ$

the hemispherical geometry of the array, while performing electronic beam steering to receive signals coming from low elevation angles, only a part of such a surface that determines the active antenna elements is present (see the right part of Fig. 7), resulting in a smaller number of active antenna elements. As the elevation angle increases, the surface centered at the spacecraft direction and angular size of $2\theta_{\text{cov}}$ becomes completely present on a hemisphere (see the left part of Fig. 7), which leads to a larger number of active antenna elements and a higher antenna gain consequently. Hence, the maximum coverage angle $\theta_{\text{cov}}$ is then adjusted such that the antenna gain achieved decreases as the elevation angle increases and the slope of decreasing fits into the normalized range loss to avoid an unnecessary margin as in the case of a tracking antenna.

In the simulations, initially a constant maximum coverage angle $\theta_{\text{cov}} = 15^\circ$ is set. For each sample on the flight path, we compare the gain of the hemispherical antenna array obtained using $\theta_{\text{cov}} = 15^\circ$ normalized by the maximum required gain of $46$ dBi with the corresponding normalized range loss. If the normalized range loss is bigger than the normalized antenna gain, the maximum coverage angle $\theta_{\text{cov}}$ is increased until the resulting normalized antenna gain is larger than or equal to the normalized range loss. In the end, the maximum coverage angle $\theta_{\text{cov}}$ is adjusted to range from $90^\circ$ to $15^\circ$ along the flight path as the elevation angle increases, which results in the adaptation of the number of active antenna elements.

Note that in Fig. 6, starting from the elevation angle of around $50^\circ$, the normalized antenna gain is larger than the normalized range loss. The reason is that for the elevation angle larger than $50^\circ$, the initially set maximum coverage angle $\theta_{\text{cov}} = 15^\circ$ already leads to a higher normalized antenna gain compared to the normalized range loss. It means that by decreasing $\theta_{\text{cov}}$, the curve of the normalized antenna gain fits even better to that of the normalized range loss. Still, it should be noted that the goal of the antenna array design is to keep the normalized antenna gain not lower than the normalized range loss and meanwhile to reduce the unnecessary margin compared to a tracking antenna, i.e., the curve of the normalized antenna gain of the designed antenna array should be located in the region between the curve of the normalized range loss and the horizontal curve representing the normalized gain of a tracking antenna.

In addition to the normalized antenna gain and the normalized range loss, the adjusted number of active antenna elements is also illustrated in Fig. 6 (see the Y-axis on the right-hand side of the figure). It is then concluded that the number of the active antenna elements is proportional to the corresponding antenna gain. It should be noted that by employing directive antenna elements instead of the omnidirectional ones, the total number of antenna elements as well as the number of active ones can be further reduced.

In Fig. 8, we present the cross-section of the beam patterns of the aforementioned hemispherical array when the beams are steered to direction $(\theta_{\text{sat}}, \phi_{\text{sat}})$ of $(5.058^\circ, 153.46^\circ)$, $(30.044^\circ, 150.221^\circ)$, and $(80.014^\circ, 83.206^\circ)$ along the flight path referred to in the previous text. The setting for the hemispherical array and the adaptation of the maximum coverage angle are the same as described for Fig. 6. We observe in

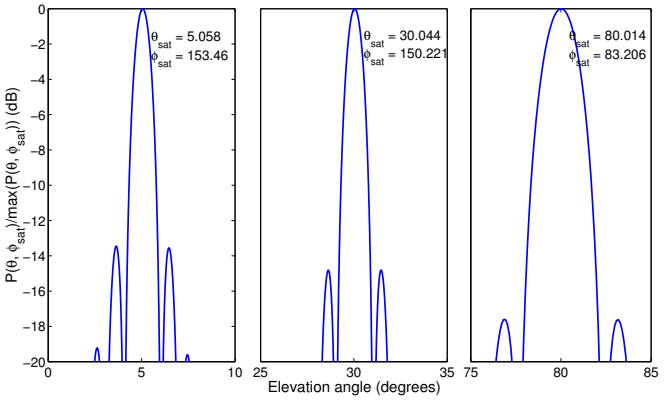


Fig. 8. Beam patterns of a hemispherical array with 82177 antenna elements in total and the number of active elements adjusted according to the normalized range loss

the beam patterns that for lower elevation angles where the number of active antenna elements is adjusted to provide a higher gain, the main beam is narrower compared to that of a higher elevation angle.

Furthermore, in Fig. 9, we present simulation results for a 5-face faceted array with a zenith face where the number of active antenna elements on the active sub-array is also adjusted to fit the normalized antenna gain to the normalized range loss. The same ascending TerraSAR-X contact over the ground

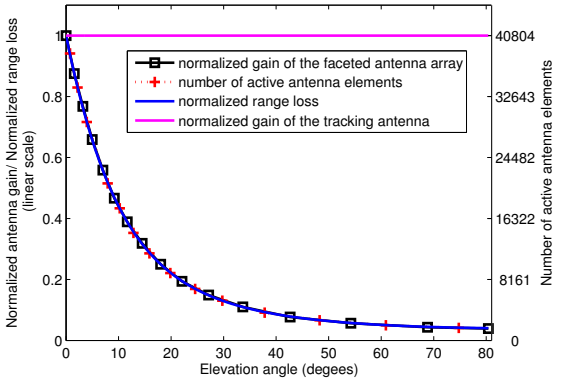


Fig. 9. Normalized array gain of a 5-face faceted array and the number of active antenna elements adjusted according to the normalized range loss

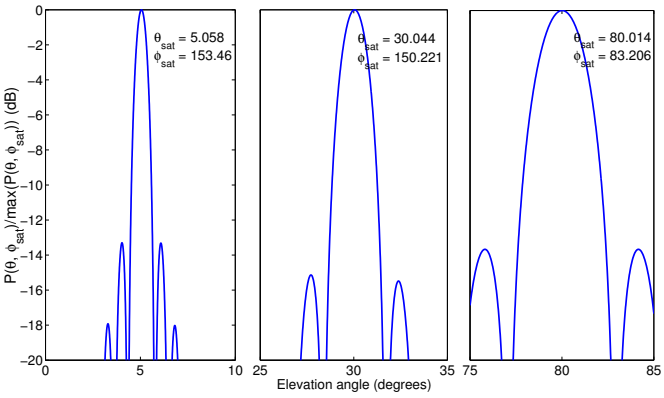


Fig. 10. Beam patterns of a 5-face faceted array with a zenith face

station Kiruna as mentioned for the case of the hemispherical array at the beginning of this section is considered. In order to achieve the required gain of 46 dBi at 0° elevation, the total number of omnidirectional antenna elements equipped on a sub-array is fixed to 40100. These antenna elements are distributed on a rectangular grid with the spacings $D = d = \frac{\lambda}{2}$ to completely avoid grating lobes. Note that the simulations are performed in a single-mission scenario, which means that only one sub-array of the 5-face faceted array is switched on at a time. For each sample of the flight path, we compare the normalized antenna gain to the normalized range loss and decrease the number of active antenna elements if the former is larger than the latter. It can be observed that the curve of the normalized antenna gain fits perfectly to that of the normalized range loss. Therefore, the goal of the antenna array design is fulfilled, and an unnecessary margin is avoided. Also, the curve for the number of active antenna elements presented in Fig. 9 (see the Y-axis on the right of the figure) indicates that the number of the active antenna elements is proportional to the corresponding antenna gain. Similar to the case of the hemispherical array, the array size can be further reduced by replacing omnidirectional antenna elements by directive ones. The beam patterns of such a 5-face faceted array with a zenith face are also shown in Fig. 10 when the beams are steered to direction $(\theta_{\text{sat}}, \phi_{\text{sat}})$ of $(5.058°, 153.46°)$, $(30.044°, 150.221°)$, and $(80.014°, 83.206°)$. The setting of this faceted array, the adaptation of the active antenna elements, and the flight path are the same as aforementioned. It can also be seen that for lower elevation angles where the number of active antenna elements on the active sub-array is adjusted to provide a higher gain, the main beam is narrower compared to that of a higher elevation angle.

## VI. Conclusion

In this work, we investigate electronic beam steering via antenna arrays as a substitute for large parabolic tracking antennas at satellite ground stations. Mainly focusing on two array geometries, faceted arrays and hemispherical arrays, we present a thorough analysis of the array size, antenna element distribution and spacing as well as the radiation properties. The concept of an optimized array design is developed by adjusting the number of active antenna elements for both array geometries such that the normalized array gain fits into the variation of the normalized range loss across the whole range of the elevation angles. In addition, the array optimization is carried out in simulations. The numerical results show that the goal of the array design is fulfilled, rendering the concept of replacing large reflector antennas by electronic beam steering via antenna arrays more convincing.

For future work, directive antenna elements will be employed, and the optimization of the antenna array directivity in such a case will be investigated. To further exploit the advantages of the antenna arrays, the interference caused by ground transmissions at low elevation angles will be taken into account, and interference-avoiding beamformers, such as the Generalized Sidelobe Canceller, can be employed. Moreover, in the presence of erroneous knowledge of the spacecraft position, e.g., caused by the refraction effect in the atmosphere, we will investigate the automatic electronic tracking as a local refinement to compensate for these errors. Implementation issues of the proposed approach will be further discussed as well.

## References


[1] G. Knittle, "Choosing the number of faces of a phased-array antenna for hemisphere scan coverage," *IEEE Trans. on Antennas and Propagation*, vol. AP-13 (6), pp. 878 - 882, Nov. 1965.

[2] J. L. Kmetzo, "An analytical approach to the coverage of a hemisphere by N planar arrays," *IEEE Trans. on Antennas and Propagation*, vol. AP-15 (3), pp. 367-371, May 1967.

[3] H. L. Van Trees, *Optimum Array Processing.* Wiley, New York, 2002.

[4] L. Josefsson and P. Persson, *Conformal Array Antenna Theory and Design.* Piscataway, NJ: IEEE Press, 2006.

[5] D. L. Sengupta, T. M. Smith, and R. W. Larson, "Radiation characteristics of a spherical array of circularly polarized elements," *IEEE Trans. on Antennas and Propagation*, vol. AP-16(1), Jan. 1968.

[6] M. Hoffman, "Convention for the analysis of spherical arrays," *IEEE Trans. on Antennas and Propagation*, vol. AP-11, pp. 390-393, July 1963.

[7] E. D. Sharp, "A triangular arrangement of planar-array elements that reduces the number needed," *IEEE Trans. on Antennas and Propagation*, vol. AP-9, pp. 126-129, March 1961.

[8] B. Tomasic, J. Turtle, S. Liu, R. Schmier, S. Bharj, and P. Oleski, "The geodesic dome phased array antenna for satellite control and communication - subarray design, development and demonstration," in *Proc. IEEE International Symposium on Phased Array System and Technology 2003*, Boston, Oct. 2003.

[9] J. Prenis, *The Dome Builder's Handbook.* Running Press, Philadelphia Pennsylvania, 1973.